JOURNAL OF THE AMERICAN CHEMICAL SOCIETY
ARTICLE
pubs.acs.org/JACS

Size-Tunable Silicon/Iron Oxide Hybrid Nanoparticles with Fluorescence, Superparamagnetism, and Biocompatibility

Keisuke Sato,*[,†] Shinobu Yokosuka,[‡] Yasunori Takigami,[‡] Kenji Hirakuri,[‡] Kouki Fujioka,[§] Yoshinobu Manome,[§] Hiroaki Sukegawa,[∥] Hideo Iwai,[⊥] and Naoki Fukata[#,▽]

[†]Department of Physics, University of Bologna, Viale Berti Pichat 6/2, 40127 Bologna, Italy
[‡]Department of Electrical and Electronic Engineering, Tokyo Denki University, 2-2 Kanda-nishiki, Chiyoda-ku, Tokyo 101-8457, Japan
[§]Department of Molecular Cell Biology, Jikei University School of Medicine, 3-25-8 Nishi-shimbashi, Minato-ku, Tokyo 105-8461, Japan
[∥]Magnetic Materials Center, and [⊥]Materials Analysis Station, National Institute for Materials Science, 1-2-1 Sengen, Tsukuba, Ibaraki 305-0047, Japan
[#]International Center for Materials Nanoarchitectonics, National Institute for Materials Science, 1-1 Namiki, Tsukuba, Ibaraki 305-0044, Japan
[▽]PRESTO, Japan Science and Technology Agency, 4-1-8 Honcho, Kawaguchi, Saitama 332-0012, Japan

Supporting Information

ABSTRACT: Magnetic/fluorescent composite materials have become one of the most important tools in the imaging modality *in vivo* using magnetic resonance imaging (MRI) monitoring and fluorescence optical imaging. We report herein on a simplified procedure to synthesize hybrid nanoparticles (HNPs) that combine silicon and magnetic iron oxides consisting of magnetite (Fe_3O_4) and maghemite (γ-Fe_2O_3). Intriguingly, our unique synthetic approach can control magnetic and optical behaviors by reducing the particle size, demonstrating that the HNPs with the mean diameter of 3.0 nm exhibit superparamagnetic behavior and green fluorescence in an aqueous solution, ambient air, and a cellular environment, whereas the HNPs with the mean diameter more than 5.0 nm indicate ferromagnetic behavior without fluorescence. Additionally, both HNPs with different diameters possess excellent magnetic responsivity for external applied magnetic field and good biocompatibility due to the low cytotoxicity. Our biocompatible HNPs with the superparamagnetism can provide an attractive approach for diagnostic imaging system *in vivo*.

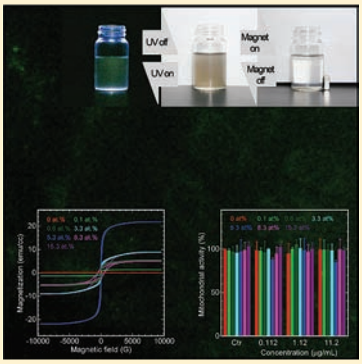

■ INTRODUCTION

Real-time diagnostic imaging system *in vivo* using fluorescent materials is important technique to detect a variety of information in living body, for instance, the tracking of fluorescently labeled biological cell migration, the diagnosis of metastatic process by the proliferation of advanced carcinoma, and the observation of bloodstream and the identification of sites for heart disease and cerebrovascular disease.[1] In such cases, the optical and the toxicological properties of fluorescent materials are absolutely critical. Conventional fluorescent materials, including organic-based dyes,[2] fluorescent proteins[3] and cadmium (Cd)-based nanoparticles (NPs), i.e., cadmium selenate and cadmium sulfide,[1a] possess specific aspects, such as high fluorescence quantum yield (QY) and size-tunable fluorescence based on quantum confinement effect.[4] However, they have been also found to have poor photostability and/or high toxicity.[5] In particular, the toxicological issue of Cd in physiological and human ecological environments is extremely serious because the Cd-ions released from the core of optically illuminated NPs are well-known to induce cell damage and might actually cause the extinction of biological system.[6] Such a serious problem has triggered the continual and urgent development of NPs consisting of nontoxic and safe materials alternative to Cd.

Fluorescent silicon NPs (Si-NPs) have shown tremendous potential as high fluorescence QY,[7] size-dependent multicolor fluorescence by the quantum confinement effect,[8] high photostability in an aqueous solution and an ambient air,[9] good biocompatibility[10] and easy modification to couple with biomolecules.[11] Intriguingly, the superior advantages of Si-NPs are nontoxic properties because they are composed of nontoxic elements and have little environmental impact.[12] Especially, the low cytotoxicities of Si-NPs stand out even after the light irradiation, leading to high cytotoxicities for the Cd-based NPs.[13] Such Si-NPs have been expected as next-generation materials alternatives to organic-based dyes, fluorescent proteins and Cd-based NPs. Further functional enhancements to the Si-NPs are indeed attractive for a broad range of practical biomedicine applications. For instance, formulations containing Si-NPs and magnetic NPs would allow not only the contrast agents of magnetic resonance imaging

Received: March 18, 2011
Published: October 12, 2011

dx.doi.org/10.1021/ja202466m | *J. Am. Chem. Soc.* 2011, 133, 18626–18633

(MRI), and the diagnosis and the enucleation of tumor using MRI monitoring for the noninvasive and nondestructive imaging modality *in vivo* but also the controlled transport and the egestion of NPs circulating in living body by applying external magnetic field. In particular, hybrid composite nanomaterials that combine the Si-NPs, the magnetic NPs and the anticancer drug doxorubicin (DOX) might attract attention for drug targeting techniques, including diagnosis of administration route and biodistribution of drugs using MRI monitoring, and controlled delivery and effective administration of drugs by applying external magnetic field. Therefore, the significant advantage of this approach is that the hybrid nanomaterials with both optical and magnetic functions containing Si-NPs and magnetic NPs can be made the diagnosis of lesion location, such as cancer cells and/or tumor, either using fluorescence optical imaging during performing the surgery, due to the limitation of penetration capability of visible fluorescence through the deeper living tissue, or using MRI monitoring before and after performing the surgery for the real-time imaging modality *in vivo*.

Herein, we became successful to demonstrate the synthesis of hybrid nanoparticles (HNPs) that combine Si and magnetic materials. We selected magnetic iron oxides, including magnetite (Fe_3O_4) and maghemite (γ-Fe_2O_3), as magnetic materials because they are well-known to be ferromagnetic materials[14] and have been widely used in biomedicine applications, such as MRI diagnosis[15] and targeted drug delivery system.[16] Intriguingly, the obtained HNPs can be tuned the optical and the magnetic behaviors by reducing the size, i.e., superparamagnetic substance with green fluorescence in an aqueous solution, an ambient air and a cellular environment, and ferromagnetic substance without fluorescence for the HNPs with the mean diameter of 3.0 nm and more than 5.0 nm, respectively. Furthermore, the important advantages of both HNPs with different diameter are excellent magnetic responsivity for external applied magnetic field, indicating the rapid movement toward the applied commercial neodymium magnet (350 mT; 3500 G) in a short period of time. Additionally, they also possess good biocompatibility due to the high viabilities of HeLa cells, derived from the human cervical cancer cell line, stained with the HNPs. Thus, our biocompatible HNPs would become a promising candidate for future practical biomedicine applications because they have considerable potential for the contrast agents of diagnostic imaging system *in vivo*, including MRI monitoring and fluorescence optical imaging, and the magnetic-field-guided targeting in living body.

■ EXPERIMENTAL SECTION

Synthesis of HNPs. The HNPs were performed by the combination of radio frequency (rf) magnetron sputtering process using a Canon Anelva SPF-210B and subsequent rapid thermal annealing process at high temperature using an Ulvac-Rico QHC-P410CP as follows. In the sputtering process in an argon (Ar) atmosphere at a gas pressure of 10 Pa and a rf power of 200 W for 120 min, excess Si atoms and iron oxide molecules, such as Fe_3O_4 and/or Fe_2O_3, were uniformly introduced in the 2-μm-thick oxide matrix by codeposition of composite targets consisting of Si chips of 5×5 mm^2 in size (Type p, crystal axis (100) and resistivity of 1−10 Ωcm, Ferrotec Silicon Co.)/magnetite chips of 5×5 mm^2 in size (purity more than 99.9%, Furuuchi Chemical Co.)/silica disk with 100 mm diameter (purity more than 99.99%, Furuuchi Chemical Co.). Under this process, the number of Si chips was fixed at 36 pieces, while the number of magnetite chips varied from 0 to 18 pieces. In next annealing process, at temperature of 1100 °C in an Ar atmosphere for 60 min, the precipitation of excess Si atoms and iron oxide molecules was simultaneously carried out in thick oxide matrix, and then iron oxide molecules were combined with excess Si atoms during the NP growth, resulting in the formation of HNPs. Under these procedures, the Fe content constituting magnetic iron oxide in the HNPs, estimated using electron probe microanalysis (EPMA) measurement, were controlled from 0 to 0.1, 0.6, 3.3, 5.3, 8.3, 15.3 at.% with the increase in the number of magnetite chips from 0 to 1, 2, 4, 8, 10, 18 pieces, respectively. To form the individual HNPs for the utilization in biomedicine applications, the obtained HNPs with different Fe content were then extracted from thick oxide matrix by treatment in a steam of 46 vol.% hydrofluoric (HF) acid solution (Wako Pure Chemical Industries Co.) at 40 °C for 2 min using a temperature-controlled bath (As One HTS-50N) and subsequent ultrasonication in an aqueous solution for 5 min using an ultrasound bath (As One US-1A). The HF acid steam and the ultrasonication processes were repeated several times to extract all of HNPs from thick oxide matrix. After that, they were spun down in an aqueous solution by a high-speed centrifugation filtration technique at 65000 rpm at 25 °C for 20 min using a Beckman Coulter Optima TLX Ultracentrifuge. The ultracentrifugation filtration process was repeated four times to remove the supernatant containing nonuniform HNPs and HF acid adsorbed on the particle surface. After the ultracentrifugation filtration process, the individual HNPs were obtained for all samples with different Fe content.

Characterizations of HNPs. High-resolution transmission electron microscopy (HRTEM) images and energy dispersive X-ray (EDX) spectra were acquired by a JEOL JEM-2100F scanning transmission electron microscope operated at an accelerating voltage of 200 kV. The samples for electron microscopy were prepared by dropping the individual HNPs with different Fe content, which were well-dispersed in ethanol, on a copper microgrid mesh. EPMA measurement was performed using a JEOL JXA-8500F field emission electron probe microanalyzer operated at a voltage of 15 kV and a current of 50 nA at room temperature. X-ray diffraction (XRD) patterns were measured at room temperature using a Rigaku RINT-Ultima3 diffractometer with Cu Kα radiation. X-ray photoelectron spectroscopy (XPS) measurement was performed using an Ulvac-Phi PHI Quantera SXM with Al Kα X-ray source at room temperature. The EPMA, the XRD and the XPS measurements were carried out for the samples in which the individual HNPs with different Fe content became uniformly exposed on the surface of substrate. Photoluminescence (PL) measurement was carried out at room temperature using a Horiba Jobin Yvon Lab RAM HR equipped with a 325-nm line of helium−cadmium (He−Cd) laser as an excitation light source. Fluorescence QY measurement was performed at room temperature using a Hamamatsu Photonics C9920−02G absolute PL-QY system equipped with integrating sphere, photonic multichannel analyzer and 313-nm line of xenon lamp. The fluorescence QY of each NP was estimated by comparing the integrated emission intensity relative to Rhodamine 6G dye solution as reference fluorescent dye. Absorption measurement was performed using a JASCO V-570 UV/vis/NIR spectrophotometer at room temperature. The PL, the fluorescence QY and the absorption measurements were carried out for the samples in which the individual HNPs with different Fe content were well-dispersed in an aqueous solution. Magnetization versus applied magnetic field (*M-H* curves) measurement was measured at room

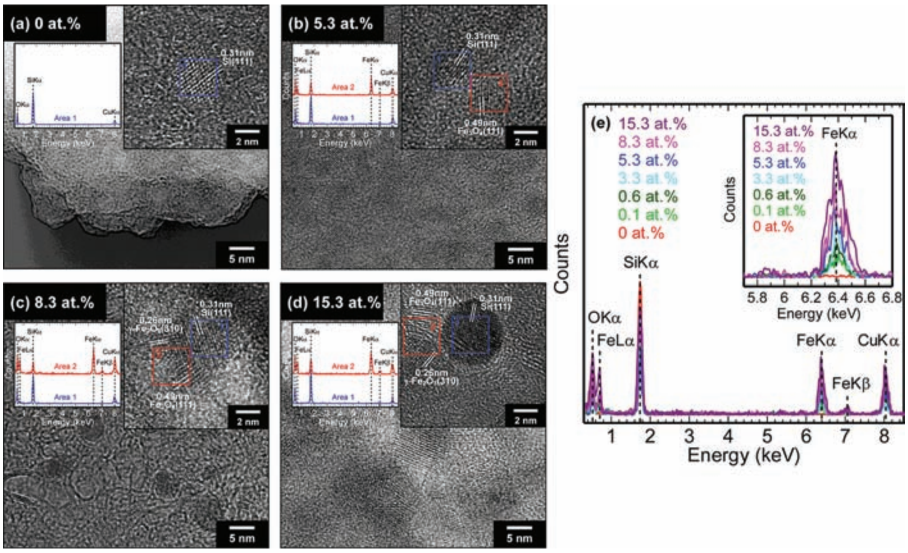

Figure 1. Plain-view HRTEM images, highly magnified HRTEM images (right of inset), and EDX spectra of boxed area 1 and 2 (left of inset) of (a) Si-NPs without magnetic iron oxide (Fe content of 0 at. %), and HNPs with Fe content of (b) 5.3 at. %, (c) 8.3 at. %, and (d) 15.3 at. %. (e) EDX spectra and magnification of Fe Kα peak (inset) of single Si-NP and single HNP with different Fe content.

temperature using a LakeShore 7403 vibrating sample magnetometer (VSM). The *M-H* measurement was carried out for the samples in which the individual HNPs with different Fe content became uniformly exposed on the surface of substrate.

Uptake of HNPs into the HeLa cells. One $\times 10^4$ cells of HeLa cell lines, which are sensitive to cytotoxicity assay, were seeded in each well of 96 well-micropalate and were incubated for 48 h at 37 °C and 5% CO_2 atmosphere. After incubation, the individual HNPs with different Fe content were added into each well in the particle concentration ranging from 0.112 to 11.2 μg/mL and were further cocultured for 48 h at 37 °C and 5% CO_2 atmosphere. Thereafter, the cells stained with each HNP were washed thrice with Dulbecco's phosphate-buffered saline (DPBS).

Fluorescence imaging and cytotoxicity assay of HeLa cells stained with the HNPs. The HeLa cells stained with the individual HNPs with different Fe content were imaged using a Keyence BZ-9000 fluorescent microscope equipped with a mercury lamp with an excitation filter at 480 nm to ensure the uptake of HNPs into the cells. For the cytotoxicity assay of HNPs, the cell viability test was performed using a Dojindo Cell Counting Kit-8 (CCK-8). The CCK-8 solution was added into each well and was incubated for 4 h at 37 °C. After incubation, soluble formazan was formed by reducing soluble tetrazolium salt (WST-8) in the CCK-8 due to high mitochondrial dehydrogenase activity in vital cells. The optical absorbance of soluble formazan was measured at 450 nm using a BioRad 680XR microplate reader ($n = 6$), and the cell viability was calculated as the ratio of the optical absorbance value of cells with each HNP to those of control cells without NPs.

RESULTS AND DISCUSSION

For characterization of the structures and the sizes of individual Si-NPs without magnetic iron oxide, i.e., Fe content of 0 at. %, and individual HNPs with different Fe content, the plain-view HRTEM analysis was employed, as shown in Figure 1a–d. The HRTEM micrograph of each HNP clearly indicates the presence of the lattice fringes due to crystalline magnetic iron oxide and crystalline Si (right of inset of Figure 1b–d), whereas the HRTEM micrograph of Si-NPs demonstrates only the lattice fringes due to crystalline Si (right of inset of Figure 1a). The lattice fringes of crystalline magnetic iron oxide correspond to (111) planes of cubic crystalline magnetite with a proper lattice spacing of 0.49 nm[17] and (310) planes of cubic crystalline maghemite with a proper lattice spacing of 0.26 nm[18] (right of inset of Figure 1b–d). Differently, the lattice fringes of crystalline Si correspond to (111) planes of cubic crystalline Si with a proper lattice spacing of 0.31 nm[19] (right of inset of Figure 1a–d). The lattice fringes due to the crystalline magnetic iron oxide are found to be present on/around the surface of the lattice fringes due to the crystalline Si for all HNPs. The compositional architecture of magnetic iron oxide and Si in their corresponding HNPs is also supported by EDX analysis attached to the TEM apparatus. The EDX spectra of the boxed area 1 and 2 (right of inset of Figure 1b–d) in the lattice fringes due to the crystalline Si and the crystalline magnetic iron oxide, respectively, for all HNPs are given in left of inset of Figure 1b–d. The EDX spectra are also compared to that of the boxed area 1 for Si-NPs (left of inset of Figure 1a). The EDX spectra derived from the O Kα line, the Fe Lα line, the Fe Kα line, and the Fe Kβ line corresponding to magnetic iron oxide are detected only in the boxed area 2 for all HNPs. The EDX spectra of the boxed area 2 in all HNPs also show the peaks derived from the surface oxide layer consisting of the O Kα line and the Si Kα line. The signal of the surface oxide layer comes from the surface region of the lattice fringes due to the crystalline Si for all HNPs. In contrast, the EDX spectra of the boxed area 1 in all HNPs and Si-NPs exhibit only the peaks derived from the O Kα line and the Si Kα line, indicating the presence of Si and its surface oxide layer. Therefore, the elemental variation of the boxed area 1 and 2 in all HNPs by EDX is consistent with the observations made by HRTEM images. The peak derived from the Cu Kα line is also detected for the boxed area 1 and 2 in all HNPs and Si-NPs. The detection of the Cu Kα line is caused by the copper microgrid mesh, which is used for the HRTEM observation. Moreover, the variation of the intensity of Fe-related peak observed from a single HNP with different Fe content is in good agreement with the Fe content, as shown in Figure 1e

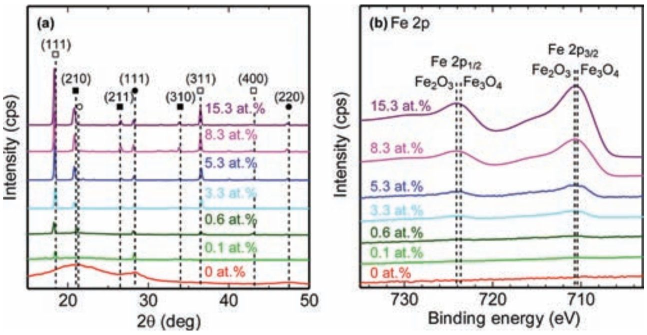

Figure 2. (a) XRD patterns and (b) Fe 2p core-level XPS spectra of Si-NPs without magnetic iron oxide (Fe content of 0 at. %) and HNPs with different Fe content. Each symbol ○, ●, □, and ■ in part a represents the diffraction peaks of amorphous silica, crystalline Si, crystalline magnetite, and crystalline maghemite, respectively.

and the inset of Figure 1e. From the above HRTEM and EDX results, it is clarified that all HNPs prepared in this study are composed of Si/magnetic iron oxide hybrid structures. Regarding the sizes of HNPs with different Fe content, the mean diameters of HNPs having low Fe content, i.e., Fe content less than 5.3 at. %, are estimated to be 3.0 nm with standard deviation of ±0.9 nm by measuring the diameters of lots of HNPs in the TEM images (Figure 1b). This mean diameter is almost the same as that, 3.0 ± 0.7 nm, of Si-NPs (Figure 1a). As the Fe content is increased from 5.3 to 8.3 at. %, the mean diameter also become larger from 3.0 ± 0.9 nm to 5.0 ± 1.4 nm (Figure 1c). Finally, the HNPs with Fe content of 15.3 at. % have the mean diameter of 8.0 ± 2.0 nm (Figure 1d). Such size-tunable HNPs have relatively good monodispersity, and no aggregation of them is observed, as can be seen in Figure 1b−d.

To further support the crystalline structures and the chemical compositions of Si-NPs and HNPs with different Fe content, the XRD and the XPS analyses were performed at room temperature, as shown in Figure 2a,b. The XRD patterns of all HNPs consist of diffraction peaks derived from the cubic phase of crystalline magnetite with space group of *Fd*3*mZ* (227)[20] ((111), (311), and (400) lattice planes corresponding to symbol □ in Figure 2a), the cubic phase of crystalline maghemite with space group of $P4_332$ (212)[21] ((210), (211), and (310) lattice planes corresponding to symbol ■ in Figure 2a), and the diamond-structured cubic phase of crystalline Si[19a] ((111) and (220) lattice planes corresponding to symbol ● in Figure 2a). Moreover, the broad diffraction peak derived from the amorphous silica[19a] (symbol ○ in Figure 2a) corresponding to surface oxide regions is slightly observed from all HNPs. On the other hand, no such diffraction peaks derived from the crystalline magnetite and the crystalline maghemite are detected for the Si-NPs, clearly showing only the diffraction peaks derived from the crystalline Si and the amorphous silica. For the XPS characterization, the peaks of Fe 2p core-level having splitting components of Fe $2p_{1/2}$ and Fe $2p_{3/2}$, due to the spin−orbit coupling, are observed from all HNPs, whereas no such peaks are obtained for the Si-NPs, as shown in Figure 2b. Moreover, the line shapes of Fe $2p_{1/2}$ and Fe $2p_{3/2}$ consist of two peaks; that is, the Fe $2p_{1/2}$ line is the peaks at the binding energy of 723.6 and 724.1 eV, while the Fe $2p_{3/2}$ line is the peaks at 710.4 and 710.7 eV. The peaks at 710.4 and 723.6 eV are in good agreement with that reported in the literature for magnetite,[22] whereas the peaks at 710.7 and 724.1 eV are in good agreement with the literature for Fe_2O_3.[22,23] Additionally, no shakeup satellite line at 719.0 eV due to the Fe^{3+} in hematite (α-Fe_2O_3),[22,23] which shows antiferromagnetic behavior in magnetic property,[24] is detected for all HNPs (Figure 2b), suggesting that no hematite is present in all HNPs. Therefore, the peaks of Fe_2O_3 are probably derived from the maghemite on the basis of XRD analysis. The integrated areas of peaks derived from the magnetite and the maghemite increase proportionally to the increase in the Fe content. Above XRD and XPS results are consistent with the observations made by HRTEM images, and are further supported the presence of magnetite and maghemite in all HNPs.

Next, to demonstrate the optical properties of Si-NPs and HNPs with different Fe content, PL analysis was conducted at room temperature, as shown in Figure 3a. The PL intensity was normalized at 1 for Si-NPs and HNPs with Fe content of 0.1 at. %. The Si-NPs show red fluorescence with an emission peak wavelength at 720 nm (emission peak energy at 1.72 eV). The fluorescence QY of Si-NPs reaches up to 23%, which is almost the same as reported values for other Si−polymer core−shell NPs dispersed in solution.[9a,25] Moreover, such Si-NPs exhibit excellent photostability for at least 1 month under ultraviolet (UV) irradiation, and no significant spectral shift is observed during our experiments (Figure S1, Supporting Information). Differently, the emitted color of HNPs having Fe content less than 5.3 at. % exhibit green light with the emission peak wavelength at 540 nm (emission peak energy at 2.296 eV), confirming that such green fluorescence of their HNPs can be obtained even after the magnetic respondency. The fluorescence QY of their HNPs is closely related to the Fe content. The HNPs with Fe content of 0.1 at. % have the fluorescence QY of 6%, which is reduced to less than a quarter of that of Si-NPs. The fluorescence QY becomes progressively lower with increasing the Fe content. As the Fe content is increased from 0.1 to 5.3 at. %, the fluorescence QY is further reduced from 6 to 1.3%. Although the decrease in the fluorescence QY is particularly large, green fluorescence of HNPs with Fe content of 5.3 at. % can be sufficiently recognized even with the storage in an aqueous solution (left of Figure 3b) and in ambient air (Figure S2a, Supporting Information). Moreover, such green fluorescence of well-dispersed HNPs with Fe content of 5.3 at. % in an aqueous solution can be also seen even after the magnetic respondency. When a commercial neodymium magnet (350 mT, 3500 G) was placed behind a cuvette containing the HNPs with Fe content of 5.3 at. %, green fluorescence appears on the side of the magnet-adsorbed HNPs, while there is no conspicuous fluorescence remaining in the solution (Figure S2b, Supporting Information). This indicates that most of HNPs are strongly attracted to the side wall of cuvette by the magnet. In the application to *in vivo* imaging a 1−5% fluorescence QY has been reported to be sufficient for cell-labeling studies.[10,26] This means that our HNPs with Fe content less than 5.3 at. % can potentially be utilized for the diagnostic imaging system *in vivo*. Finally, green fluorescence seems to disappear for the HNPs with Fe content more than 8.3 at. %, indicating that the fluorescence QY is not detectable for their HNPs. The reason for the decrease in the fluorescence QY and disappearance of green fluorescence with the increase in the Fe content is described in a later section. Regarding the photostabilities of HNPs with Fe content less than 5.3 at. %, their HNPs is maintained more than 90% of their initial maximum fluorescence intensity even after a month of UV irradiation, like that of Si-NPs (Figure S1, Supporting Information). This resistance to fluorescence photobleaching of HNPs is comparable to other Si-NPs that are photostable for a prolonged

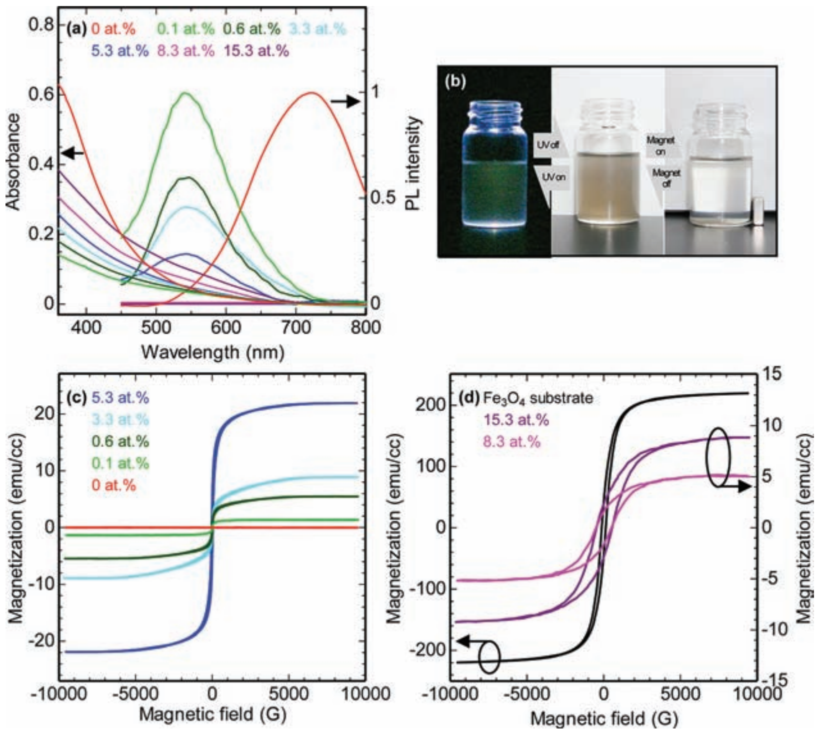

Figure 3. (a) PL and absorbance spectra of Si-NPs without magnetic iron oxide (Fe content of 0 at. %) and HNPs with different Fe content. (b) Fluorescence image (middle) before and (left) after UV light irradiation, and photograph (middle) before and (right) after magnetic respondency by a magnet for the well-dispersed HNPs with Fe content of 5.3 at. % in an aqueous solution. Magnetization ($M-H$) curves of (c) Si-NPs and HNPs with Fe content less than 5.3 at. %, and (d) HNPs with Fe content more than 8.3 at. % and magnetite substrate.

time.[25b,c,27] Therefore, the long-term photostable HNPs may become valuable for *in vivo* imaging studies.

To understand the mechanisms governing the variation of fluorescence color between the Si-NPs and the HNPs with Fe content less than 5.3 at. %, absorption analysis was also employed at room temperature, as shown in Figure 3a. The optical band gap energy corresponding to size distribution for Si-NPs and HNPs with different Fe content was estimated using the absorption coefficient analysis. The correlation among the optical band gap energy and wavelength for Si-NPs and HNPs having size distribution shown in Figure 1a−d is summarized as follows: 2.3 eV and 539 nm for 3.0 ± 0.7−0.9 nm corresponding to Si-NPs and HNPs with Fe content less than 5.3 at. %, 1.5 eV and 828 nm for 5.0 ± 1.4 nm corresponding to HNPs with Fe content of 8.3 at. %, and 1.4 eV and 885 nm for 8.0 ± 2.0 nm corresponding to HNPs with Fe content of 15.3 at. %. The optical band gap energies of HNPs with Fe content less than 5.3 at. %, which show green fluorescence, are found to have the same value as those of Si-NPs, which exhibit red fluorescence, even though the HNPs are composed of Si/magnetic iron oxide hybrid structures. This might be related to the presence of a smaller amount of magnetic iron oxide in each HNP and their uniform size distribution, as shown in Figure 1a,b,e. Therefore, this result means that no variation of fluorescence color between the Si-NPs and the HNPs with Fe content less than 5.3 at. % is attributable to the size effect. Interestingly, the difference in the energy between the optical band gap and the emission peak is different for Si-NPs and HNPs; that is, the emission peak energy of red fluorescence is at a lower value than the optical band gap energies of Si-NPs, whereas the emission peak energy of green fluorescence is almost the same value as the optical band gap energies of HNPs with Fe content less than 5.3 at. %. This result suggests that the variation of fluorescence color is most likely due to the different radiative recombination pathways for Si-NPs and HNPs. In the case of Si-NPs the surface is surrounded by the oxide layer, as identified by EDX and XRD analyses (left of inset of Figures 1a and 2a). The surface oxidation forms the Si−O bonding structure, i.e., Si═O bonds,[28] on the surfaces of Si-NPs. Additionally, the formation of such Si−O bonding structure brings about the generation of oxygen-related trap levels, which act as the radiative recombination sites of electron−hole pairs, localized within the optical band gap.[8c,9d,27] As a result, the emission peak energies of Si-NPs show a lower value than the optical band gap energy. Therefore, red fluorescence observed from the Si-NPs is closely attributable to the radiative recombination processes of electron−hole pairs through the oxygen-related trap levels within the size-dependent optical band gap after the irradiation with an excitation light above the optical band gap energy. The oxygen-related trap levels are more likely to be varying by combining Si and magnetic iron oxide; that is, the HNPs inhibit the formation of trap levels within the optical band gap, resulting in the emission peak energy being close to the optical band gap energy. As a result, the radiative recombination processes of HNPs with Fe content less than 5.3 at. % take control of interband transition from transition through the oxygen-related trap levels within the optical band gap. Therefore, green fluorescence obtained for such HNPs arises from the radiative recombination processes of electron−hole pairs in the vicinity of conduction band edge and valence band edge within the optical band gap. Consequently, the difference in the radiative recombination pathways of electron−hole pairs in the optical band gaps for Si-NPs and HNPs with Fe content less than 5.3 at. % led to the variation of fluorescence color. Moreover, the reason for the decrease in the fluorescence QY and disappearance of green fluorescence with the increase in the Fe content is as follows. Park and Sailor et al. have reported that the intensity of fluorescence from the micellar HNPs containing fluorescent quantum dots (QDs) and magnetic iron oxide NPs is decreased with increasing the ratio of magnetic iron oxide NPs to fluorescent QDs within a micelle.[29] Moreover, they have also suggested that the proximity of magnetic iron oxide NPs and other fluorescent QDs in the micellar HNPs is likely to cause fluorescence quenching through nonradiative energy. These results are in accord with our results. Therefore, the decrease in the fluorescence QY observed in this study supports the contribution of the nonradiative recombination process. The formation of nonradiative recombination levels in the HNPs might be associated with the presence of magnetic iron oxide because the increase in the Fe content results in the decrease in the fluorescence QY. That is, the magnetic iron oxide brings about the generation of Fe-related impurity levels localized within the optical band gap of HNPs. Moreover, the increased Fe content induces the expansion of Fe-related impurity levels due to the increase in the magnetic iron oxide. The Fe-related impurity levels act as nonradiative recombination sites under the recombination processes of electron−hole pairs. As a result, the recombination processes of electron−hole pairs for the HNPs with high Fe content take place both for the transition through the Fe-related trap states within the optical band gap and the transition in the vicinity of conduction band edge and valence band edge within the optical band gap; the former acts as the nonradiative recombination processes of electron−hole pairs, and the latter acts as the radiative recombination processes of electron−hole pairs. This implies that the radiative recombination probabilities of electron−hole pairs in the vicinity of each band edge, which cause green fluorescence, for the HNPs with Fe content of 5.3 at. % become lower further compared to that of 0.1 at. %, since the number of electron−hole pairs, which recombine through the Fe-related trap states, increase. Due to the reduction of radiative recombination probability, the fluorescence QY becomes progressively weaker from 6% to 1.3% with the increase in the Fe content from 0.1 to 5.3 at. %. In the case of HNPs with Fe content more than 8.3 at. %, the number of electron−hole pairs, which recombine through the Fe-related trap states, further increases. Additionally, such HNPs possess the mean diameter more than 5.0 nm, which is larger than that, 3.0 nm, of HNPs with Fe content less than 5.3 at. % and thereby have a narrower optical band gap corresponding to the infrared region, as identified by HRTEM and absorption analyses shown in Figures 1c,d and 3a, respectively. Thus, the increase in both transition processes through the Fe-related trap states and particle size is conducive to the disappearance of green fluorescence for the HNPs with Fe content more than 8.3 at. %. Regarding the improvement of fluorescence QY, some researchers have reported that the surface-coating technology using poly(acrylic acid) (PAAc) polymer is an effective tool for increasing the fluorescence QY of pure Si-NPs.[9a,25b] Indeed, the PAAc-modified pure Si-NPs have been shown the fluorescence QY, which is more than six times larger than that of unmodified ones. On the other hand, the HNPs prepared in this study contain the Fe-related impurity levels, which act as nonradiative recombination levels, within the optical band gap owing to the presence of magnetic iron oxide. Thus, the PAAc polymer coating may not be an effective tool for increasing the fluorescence QY of HNPs containing the Fe-related impurity levels, although it can increase the fluorescence QY of pure Si-NPs. To increase the fluorescence QY of HNPs consisting of Si and magnetic iron oxide, the micellar HNPs containing fluorescent QDs and magnetic iron oxide NPs, which are supported by Park and Sailor et al.,[29] and Erogbogbo, Prasad, and Swihart et al.,[30] may be more effective rather than our HNPs because the fluorescent QDs within a micelle can completely prevent the formation of Fe-related impurity levels.

For characterization of the magnetic properties of Si-NPs and HNPs with different Fe content, $M-H$ analysis was investigated at room temperature, as shown in Figure 3c,d. The shape of $M-H$ curve strongly depends on the sizes of HNPs. The HNPs having mean diameter of 3.0 nm for Fe content less than 5.3 at. % exhibit negligible coercivity (H_c) and remnant magnetization (M_r), which is typical of superparamagnetic behavior without hysteresis, whereas no such magnetization curve is obtained for the Si-NPs, as shown in Figure 3c. The H_c and M_r mean the applied magnetic field necessary to reduce the material to a zero magnetization, and the residual magnetization at a zero magnetic field after saturating its magnetization, respectively. The realization of HNPs with the superparamagnetism of 3.0 nm in size obtained in this study is particularly attractive for the widespread application in biomedicine fields because the risk forming agglomerate of HNPs is negligible at room temperature, and the HNPs can be redispersed rapidly with the removal of the magnetic field. On the other hand, the HNPs having mean diameter more than 5.0 nm for Fe content more than 8.3 at. % indicate ferromagnetic hysteresis, which has values of H_c and M_r more than 500 G and 1.6 emu/cc, respectively, as shown in Figure 3d. The value of H_c is much larger than 131 G for the magnetite substrate, which was used as the sputtering target (Figure 3d). The enhanced H_c is due to the coherent magnetization reversal by single-domain because the HNPs are composed of Si/magnetic iron oxide hybrid structures. Thus, the magnetic behaviors of our HNPs can be controlled from the ferromagnetism to the superparamagnetism by the reduction of size with the decrease in the Fe content. The variation from the ferromagnetism to the superparamagnetism is closely attributable to the small particle size and finite domain size effect[31] of magnetic components in the HNPs because of the thermal fluctuation of magnetic moment at room temperature. Moreover, the magnitude of saturation magnetization (M_s) is important to understand the magnetic responsivity of HNPs to the external magnetic field for the utilization in biomedicine applications, such as contrast agents of diagnostic imaging system *in vivo*, including MRI monitoring and fluorescence optical imaging, and magnetic-field-guided targeting in living body. The maximum values of M_s of HNPs with the superparamagnetism and the ferromagnetism are 22.2 and 9.0 emu/cc for Fe content of 5.3 and 15.3 at. %, respectively. These values of M_s are reduced more than 1 order of magnitude compared to that (220 emu/cc) of magnetite substrate (Figure 3d). The decreased M_s is probably due to the presence of a smaller amount of magnetic iron oxide in each HNP because the reduction of magnetic iron oxide leads to decrease in the net magnetic moment. Although the decrease in the M_s is particularly large, the well-dispersed HNPs, i.e., superparamagnetic substance with Fe content of 5.3 at. %, in an aqueous solution (middle of Figure 3b) can be readily and completely gathered to the wall by placing a commercial neodymium magnet (350 mT, 3500 G) outside of the cuvette within about 5 min (right of Figure 3b), indicating the excellent magnetic responsivity. After the movement of them, the suspension become clear and transparent (right of Figure 3b). Furthermore, most of them are sufficiently attracted to the upper wall through the magnet even in the situation with the cuvette turned upside down (Figure S3, Supporting Information). Such magnetic responsivity by the magnet is sufficient for the M_s over 5 emu/cc corresponding to Fe content of 0.6 and 8.3 at. % for the HNPs with the superparamagnetism and the ferromagnetism, respectively, although the collection times of them become relatively longer.

Finally, to clarify whether the HNPs exhibit good biocompatibility that can potentially be utilized for the diagnostic imaging system *in vivo*, including MRI monitoring and fluorescence optical imaging, the cellular uptake and the cell viability analyses for the HeLa cells stained with Si-NPs and HNPs with different Fe content were conducted using transmitted light imaging and fluorescence imaging, and MTT (3-[4,5-dimethyl-2-thiazolyl]-2,5-diphenyl-2*H*-tetrazolium bromide) assay, respectively, as shown in Figure 4a−c. All HNPs are well taken up by HeLa cells even with the high particle concentration, i.e., 100 μg/mL, and most of them are distributed in the cytoplasmic region, indicating that the uptake of them does not affect not only the cell morphology but also the cell viability, as shown in Figure 4a,b for the HNPs with Fe content of 5.3 at. %. The cellular uptake of HNPs might be occurring through the nonreceptor-mediated endocytosis pathway existing in the cells to enter in the cytoplasmic region because the nonreceptor-mediated endocytosis seems to be a general process occurring frequently in various cells, including HeLa cells,[32] upon ingestion of NPs without having surface-grafted agonists, i.e., folate moieties. Regarding the fluorescence imaging of HNPs after the cellular uptake, their fluorescence images show dusky-green light. In particular, green fluorescence intensities in the cells (Figure 4b) for the HNPs with Fe content of 5.3 at. %, which have the superparamagnetism and the highest M_s (Figure 3c), are relatively weak compared to those in an aqueous solution (left of Figures 3b and S2b, Supporting Information) and ambient air (Figure S2a, Supporting Information). Naturally, no such green fluorescence is quite detectable for the control, which was incubated with media without NPs. Additionally, in the cellular uptake of HNPs using a commercial neodymium magnet (350 mT; 3500 G) they cause a dramatic fall in the magnetic response in the cell culture environment, although they show good magnetic responsivity in an aqueous solution. Similar results have also been observed from the HNPs dispersed in the biological solution. When dispersed in the biological solution, such as DPBS and 0.9% physiological saline solution, for several hours, the HNPs cause the degradation of green fluorescence intensity and the lowering of magnetic response. Therefore, these results indicate that the observation of dusky green fluorescence of HNPs and the lowering of their magnetic response in the cell culture environment are probably due to the effect of salt. To protect the fluorescence and magnetic properties of HNPs from the salt, the surface chemical modification of HNPs, e.g., polymeric surface coating,[8c] is absolutely critical. He, Fan, and Lee et al. have reported that the fluorescence intensity of PAAc-modified Si-NPs is remarkably stable even after the cellular uptake.[25b] Moreover, they have also suggested that the PAAc polymer shell effectively protects the fluorescence of Si-NPs. This PAAc polymer shell might also be effective in protecting the magnetic properties of our HNPs from the salt. Therefore, we suggest that such a polymer coating is one effective tool to protect the fluorescence and magnetic properties of our HNPs from the special environment, such as an *in vivo* environment.

Regarding the biocompatibility and the cytotoxicities of Si-NPs and HNPs with different Fe contents, MTT assay was carried out under the particle concentration range from 0.112 to 11.2 μg/mL, as shown in Figure 4c. All HNPs exhibit a remarkably stable cell survival feature independently of the variation of Fe content, resulting in the high cell viability more than 85 ± 2.4% even after the incubation with 11.2 μg/mL. Such high cell viabilities of them show almost the same trend as those of control and Si-NPs. From this cell viability tendency, the 50% inhibition coefficients of all HNPs would be predicted to occur in the particle concentration, which is much higher than 11.2 μg/mL. Our findings regarding the above cytotoxicity assay clearly demonstrate that no cell viability is affected by the uptake of HNPs, suggesting that all HNPs prepared in this study are reasonably biocompatible and do not also have significant adverse effects, such as toxic effects, for future practical applications *in vivo*.

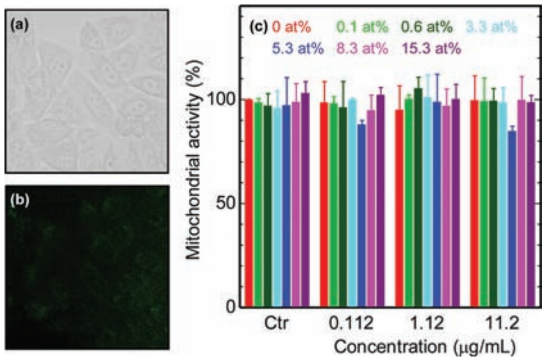

Figure 4. (a) Transmitted light image and (b) fluorescence image of HeLa cells cultured with medium containing HNPs with Fe content of 5.3 at. %. (c) MTT assay of HeLa cells incubated with media containing Si-NPs without magnetic iron oxide (Fe content of 0 at. %) and HNPs with different Fe content for the particle concentration ranging from 0.112 to 11.2 μg/mL.

■ CONCLUSIONS

We designed the HNPs that combine silicon and magnetic iron oxides consisting of magnetite and maghemite. Intriguingly, the HNPs conduce to different optical and magnetic behaviors by the reduction of size, such as the superparamagnetic substance with green fluorescence performance in an aqueous solution, an ambient air and a cellular environment, and the ferromagnetic substance without fluorescence performance for the HNPs with the mean diameter of 3.0 nm and more than 5.0 nm, respectively. Both HNPs with different diameters possess excellent magnetic responsivity for external applied magnetic field and also provide good biocompatibility due to the high viabilities of HeLa cells stained with the HNPs. Therefore, we strongly believe that our biocompatible HNPs have considerable potential for contrast agents of diagnostic imaging system *in vivo*, including MRI monitoring and fluorescence optical imaging, and the magnetic-field-guided targeting in living body. Additionally, the HNPs with the superparamagnetism of 3.0 nm in size obtained in this study would bring significant benefits to widespread biomedicine applications because they can be magnetically operated only for external applied magnetic field and can also be redispersed rapidly with the removal of magnetic field. The present approach can open up new avenues for future various optical and biotechnological applications using HNPs.

■ ASSOCIATED CONTENT

Ⓢ **Supporting Information.** Photostabilities of Si-NPs and HNPs with different Fe content, and fluorescence image and photograph after magnetic respondency of HNPs with Fe content of 5.3 at. %. This material is available free of charge via the Internet at http://pubs.acs.org.

■ AUTHOR INFORMATION

Corresponding Author

keisuke.sato@unibo.it

■ ACKNOWLEDGMENT

This work was supported by the research grant from the Konica Minolta Imaging Science Foundation, and the research grant from the Iketani Science and Technology Foundation. The safety test in this work was also supported by the Ministry of Health, Labour and welfare of Japan (H22-Chemical-Young-009).

■ REFERENCES

(1) (a) Michalet, X.; Pihand, F. F.; Bentolila, L. A.; Tsay, J. M.; Doosc, S.; Li, J. J.; Sundaresan, G.; Wu, A. M.; Gambhir, S. S.; Weiss, S. *Science* **2005**, *307*, 538–544. (b) Liu, W.; Choi, H. S.; Zimmer, J. P.; Tanaka, E.; Frangioni, J. V.; Bawendi, M. *J. Am. Chem. Soc.* **2007**, *129*, 14530–14531.

(2) (a) Ernst, L. A.; Gupta, R. K.; Mujumdar, R. B.; Waggoner, A. S. *Cytometry* **1989**, *10*, 3–10. (b) Abbott, A. J.; Amler, E.; Ball, W. J., Jr. *Biochemistry* **1991**, *30*, 1692–1701.

(3) Lippincott-Schwartz, J.; Patterson, G. H. *Science* **2003**, *300*, 87–91.

(4) Wang, S.; Jarrett, B. R.; Kauzlarich, S. M.; Louie, A. Y. *J. Am. Chem. Soc.* **2007**, *129*, 3848–3856.

(5) (a) Hardman, R. *Environ. Health Perspect.* **2006**, *114*, 165–172. (b) Rzigalinski, B. A.; Strobl, J. S. *Toxicol. Appl. Pharmacol.* **2009**, *238*, 280–288.

(6) (a) Derfus, A. M.; Chan, W. C. W.; Bhatia, S. N. *Nano Lett.* **2004**, *4*, 11–18. (b) Kirchner, C.; Liedl, T.; Kudera, S.; Pellegrino, T.; Javier, A. M.; Gaub, H. E.; Stollzle, S.; Fertig, N.; Parak, W. J. *Nano Lett.* **2005**, *5*, 331–338.

(7) (a) Zhang, X.; Neiner, D.; Wang, S.; Louie, A. Y.; Kauzlarich, S. M. *Nanotechnology* **2007**, *18*, 095601. (b) Heintz, A. S.; Fink, M. J.; Mitchell, B. S. *Adv. Mater.* **2007**, *19*, 3984–3988.

(8) (a) Godefroo, S.; Hayne, M.; Jivanescu, M.; Stesmans, A.; Zacharias, M.; Lebedev, O. I.; Tendeloo, G. V.; Moshchalkov, V. V. *Nat. Nanotechnol.* **2008**, *3*, 174–178. (b) Kang, Z.; Liu, Y.; Tsang, C. H. A.; Ma, D. D. D.; Fan, X.; Wong, N.-B.; Lee, S.-T. *Adv. Mater.* **2009**, *21*, 661–664. (c) Sato, K.; Fukata, N.; Hirakuri, K.; Murakami, M.; Shimizu, T.; Yamauchi, Y. *Chem.—Asian J.* **2010**, *5*, 50–55.

(9) (a) Li, Z. F.; Ruckenstein, E. *Nano Lett.* **2004**, *4*, 1463–1467. (b) Sato, K.; Hirakuri, K. *J. Appl. Phys.* **2005**, *97*, 104326. (c) Hiruoka, M.; Sato, K.; Hirakuri, K. *J. Appl. Phys.* **2007**, *102*, 024308. (d) Sato, K.; Tsuji, H.; Hirakuri, K.; Fukata, N.; Yamauchi, Y. *Chem. Commun.* **2009**, 3759–3761.

(10) Erogbogbo, F.; Yong, K.-T.; Roy, I.; Xu, G.; Prasad, P. N.; Swihart, M. T. *ACS Nano* **2008**, *2*, 873–878.

(11) Warner, J. H.; Hoshino, A.; Yamamoto, K.; Tilley, R. D. *Angew. Chem., Int. Ed.* **2005**, *44*, 4550–4554.

(12) Park, J.-H.; Gu, L.; Maltzahn, G.; Ruoslahti, E.; Bhatia, S. N.; Sailor, M. J. *Nat. Mater.* **2009**, *8*, 331–336.

(13) Fujioka, K.; Hiruoka, M.; Sato, K.; Manabe, N.; Miyasaka, R.; Hanada, S.; Hoshino, A.; Tilley, R. D.; Manome, Y.; Hirakuri, K.; Yamamoto, K. *Nanotechnology* **2008**, *19*, 415102.

(14) Zhou, Z.-J.; Yan, J.-J. *J. Magn. Magn. Mater.* **1992**, *115*, 87–98.

(15) (a) Lai, C.-W.; Wang, Y.-H.; Lai, C.-H.; Yang, M.-J.; Chen, C.-Y.; Chou, P.-T.; Chan, C.-S.; Chi, Y.; Chen, Y.-C.; Hsiao, J.-K. *Small* **2008**, *4*, 218–224. (b) Bardhan, R.; Chen, W.; Torres, C. P.; Bartels, M.; Huschka, R. M.; Zhao, L. L.; Morosan, E.; Pautler, R. G.; Joshi, A.; Halas, N. J. *Adv. Funct. Mater.* **2009**, *19*, 3901–3909.

(16) (a) Chen., L.-B.; Zhang, F.; Wang, C.-C. *Small* **2009**, *5*, 621–628. (b) Chandra, S.; Mehta, S.; Nigam, S.; Bahadur, D. *New J. Chem.* **2010**, *34*, 648–655.

(17) (a) Wang, H.; Chen, Q.-W.; Sun, Y.-B.; Wang, M.-S.; Sun, L.-X.; Yan, W.-S. *Langmuir* **2010**, *26*, 5957–5962. (b) Hui, C.; Shen, C.; Tian, J.; Bao, L.; Ding, H.; Li, C.; Tian, Y.; Shi, X.; Gao, H.-J. *Nanoscale* **2011**, *3*, 701–705.

(18) (a) Morales, M. P.; Veintemillas-Verdaguer, S.; Montero, M. I.; Serna, C. J. *Chem. Mater.* **1999**, *11*, 3058–3064. (b) Serna, C. J.; Bødker, F.; Mørup, S.; Morales, M. P.; Sandiumenge, F.; Veintemillas-Verdaguer, S. *Solid State Commun.* **2001**, *118*, 437–440.

(19) (a) Sato, K.; Izumi, T.; Iwase, M.; Show, Y.; Morisaki, H.; Yaguchi, T.; Kamino, T. *Appl. Surf. Sci.* **2003**, *216*, 376–381. (b) Sun, X.-H.; Wong, N.-B.; Li, C.-P.; Lee, S.-T.; Kim, P.-S. G.; Sham, T.-K. *Chem. Mater.* **2004**, *16*, 1143–1152.

(20) Wechsler, B. A.; Lindsley, D. H.; Prewitt, C. T. *Am. Mineral.* **1984**, *69*, 754–770.

(21) Shmakov, A. N.; Kryukova, G. N.; Tsybulya, S. V.; Chuvilin, A. L.; Solovyeva, L. P. *J. Appl. Crystallogr.* **1995**, *28*, 141–145.

(22) Kim, K. J.; Moon, D. W.; Lee, S. K.; Jung, K.-H. *Thin Solid Films* **2000**, *360*, 118–121.

(23) Pan, L.; Zhang, G.; Fan, C.; Qiu, H.; Wu, P.; Wang, F.; Zhang, Y. *Thin Solid Films* **2005**, *473*, 63–67.

(24) Dimitrov, D. V.; Hadjipanayis, G. C.; Papaefthymiou, V.; Simopoulos, A. *IEEE Trans. Magn.* **1997**, *33*, 4363–4366.

(25) (a) Rosso-Vasic, M.; Spruijt, E.; Van Lagen, B.; De Cola, L.; Zuilhof, H. *Small* **2008**, *4*, 1835–1841. (b) He, Y.; Kang, Z.-H.; Li, Q.-S.; Tsang, C. H. A.; Fan, C.-H.; Lee, S.-T. *Angew. Chem., Int. Ed.* **2009**, *48*, 128–132. (c) He, Y.; Su, Y.; Yang, X.; Kang, Z.; Xu, T.; Zhang, R.; Fan, C.; Lee, S.-T. *J. Am. Chem. Soc.* **2009**, *131*, 4434–4438.

(26) Zimmer, J. P.; Kim, S. W.; Ohnishi, S.; Tanaka, E.; Frangioni, J. V.; Bawendi, M. G. *J. Am. Chem. Soc.* **2006**, *128*, 2526–2527.

(27) Lin, S.-W.; Chen, D.-H. *Small* **2009**, *5*, 72–76.

(28) (a) Gole, J. L.; Dudel, F. P.; Grantier, D.; Dixon, D. A. *Phys. Rev. B* **1997**, *56*, 2137–2153. (b) Wolkin, M. V.; Jorne, J.; Fauchet, P. M.; Allan, G.; Delerue, C. *Phys. Rev. Lett.* **1999**, *82*, 197–200. (c) Luppi, M.; Ossicini, S. *Phys. Rev. B* **2005**, *71*, 035340.

(29) Park, J.-H.; Von Maltzahn, G.; Ruoslahti, E.; Bhatia, S. N.; Sailor, M. J. *Angew. Chem., Int. Ed.* **2008**, *47*, 7284–7288.

(30) Erogbogbo, F.; Yong, K.-T.; Hu, R.; Law, W.-C.; Ding, H.; Chang, C.-W.; Prasad, P. N.; Swihart, M. T. *ACS Nano* **2010**, *4*, 5131–5138.

(31) (a) Lu, A.-H.; Salabas, E. L.; Schuth, F. *Angew. Chem., Int. Ed.* **2007**, *46*, 1222–1244. (b) Dahal, N.; Chikan, V. *Chem. Mater.* **2010**, *22*, 2892–2897.

(32) Olson, J. K.; Grose, C. *J. Virol.* **1997**, *71*, 4042–4054.